

1 *Conference Proceedings Paper*

2 **Numerical simulation of nocturnal ozone increase in** 3 **Metropolitan Area of São Paulo**

4 **Viviana Vanesa Urbina Guerrero**¹, **Marcos Vinicius Bueno de Morais**^{2,*}, **Edmilson Dias de**
5 **Freitas**¹, and **Leila Droprinchinski Martins**³

6 ¹ Instituto de Astronomia, Geofísica e Ciências Atmosféricas, Universidade de São Paulo, São Paulo 05508-
7 090, Brazil; viviana.urbina@gmail.com (V.V.U.G); edmilson.freitas@iag.usp.br (E.D.F.)

8 ² Departamento de Obras Civiles, Facultad de Ciencias de la Ingeniería, Universidad Católica del Maule, Av.
9 San Miguel 3605, Talca 3480112, Chile; bmarcos@ucm.cl

10 ³ Department of Chemistry, Federal University of Technology - Paraná, Pioneiros Avenue, 3131, 86036-370,
11 Londrina-PR, Brazil.

12 * Correspondence: bmarcos@ucm.cl; Tel.: +56-712-203-566(M.V.B.M)

13 Received: date; Accepted: date; Published: date

14 **Abstract:** In large cities, pollution can not only cause deaths and illnesses due to exposure of people
15 to it, but it can also reduce visibility on days of high atmospheric stability and high emission of
16 pollutants, which can even result in vehicular accidents. Ozone is an atmospheric oxidizing gas that
17 forms in minimal amounts naturally. People's health can be affected by the ozone present in the air
18 they breathe, even in low concentrations, which can worsen preexisting diseases and increase
19 hospital admissions for respiratory diseases, especially in babies, after episodes of high pollutant
20 levels. An increase in secondary peaks during the night of this atmospheric pollutant occurs in
21 several parts of the world, but its formation depends on the local condition. In this sense, this work
22 aims to study the regional atmospheric characteristics for the nocturnal ozone formation in the
23 Metropolitan Area of São Paulo (MASP). For this, the Simple Photochemical Module (SPM) coupled
24 to the BRAMS (Brazilian Developments of Regional Atmospheric Modeling System) will be used to
25 simulate this condition for the urban region. The results showed that the secondary nocturnal
26 maximum of ozone concentrations in MASP is related to vertical transport of this pollutant from
27 higher levels of the atmosphere to the surface.

28 **Keywords:** nocturnal ozone; air quality modeling; simple photochemical modeling

29

30 **1. Introduction**

31 Pollutants are naturally present in the atmosphere due to fires, volcanic eruptions and biogenic
32 emissions; but the greatest contribution is currently associated with anthropic activities. In Latin
33 America, urban centers are in constant development and growth, generating numerous problems
34 associated with the effects of pollution [1]. In large cities, pollution can not only cause deaths and
35 illnesses due to exposure of people to it but can also reduce visibility on days of high atmospheric
36 stability and high emission of pollutants, and can even result in vehicular accidents [2–4]. Several
37 studies have shown that the meteorological condition has a great influence on the concentrations of
38 pollutants [5–9].

39 Ozone (O₃) is an atmospheric oxidizing gas that forms in very small amounts naturally. This
40 secondary photochemical pollutant is formed in the atmosphere by photo dissociation of nitrogen
41 dioxide (NO₂) by ultra-violet light. For being an oxidant pollutant, ground-level ozone concentration
42 can affect people health (especially children, elderly and people in outdoor activities), worsen pre-

43 existent diseases and increasing the number of hospitalizations by respiratory diseases in risk groups
44 [10]. Also, ozone exposure can be related to morbidity and mortality by cardiopulmonary diseases
45 [11]. In United States, ozone contributes to increase the mortality rate associated to respiratory
46 diseases, being that an increment of 10 ppb in ground-level concentrations increase in 3% death risk
47 associate to exposure [12]. Climatic change could be responsible by increase in ozone concentrations
48 and, consequently, in the number of hospital admissions and deaths associated to ozone exposure
49 [4]. Since, change in ozone concentrations are, in part, consequence of changes in the atmospheric
50 system, it is important to know which synoptic patterns are associated to singular conditions of
51 ground-level ozone concentrations.

52 During night, at very stable situations, especially under anticyclonic conditions, the increase of
53 this contaminant has been observed with a well-defined behavior [13]. In cyclonic conditions, NO_x
54 can have low due to increased ventilation, and affect O₃ concentration [14]. The magnitude and
55 frequency of nocturnal ozone peaks are generally observed in summer time, and can be associated
56 with horizontal transport processes [15]. Also, in China, the nocturnal O₃ concentration is higher in
57 suburban areas than in urban areas before it increase, reduced under the effect of vertical transport
58 [16].

59 Given the importance and the elements that influence the magnitude and frequency of nocturnal
60 ozone, this work aims to study the regional characteristics of the atmosphere of the Metropolitan
61 Area of São Paulo in the formation of secondary ozone peaks during the night. For this, regional
62 numerical modeling coupled with a chemical module will be used.

63 **2. Methodology**

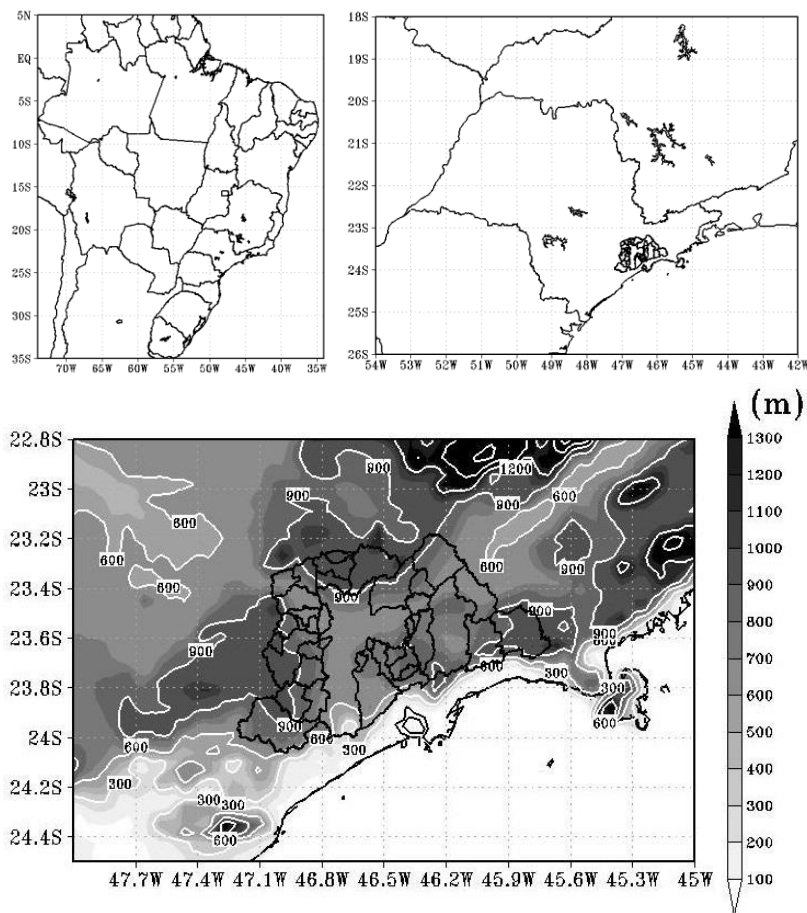
64 *2.1. Study Area*

65 The Metropolitan Area of São Paulo (MASP) is located in southeastern Brazil, in a region of
66 rugged topography (Figure 1), in which the city of São Paulo is located in the most central region
67 coinciding with the valleys of the Tietê and Pinheiros rivers, between Serra do Mar and Serra da
68 Cantareira, the latter, with elevations above 1000 m. The MASP comprises 39 municipalities and
69 concentrates almost half of the state's total population (approximately 20 million inhabitants),
70 covering an area of 8051 km² [17].

71 Given the proximity of the MASP to the coast, the surface extension of the urban area, and the
72 heat island effect seen in it make this type of thermal origin generate a significant influence on the
73 flow patterns [18] in the dispersion of pollutants. The passage of the sea breeze creates a favorable
74 condition for the dispersion of pollutants in this urban region, while days with extreme heat island
75 events generate a more stable condition on the RMSP, which may favor the accumulation of
76 pollutants[9]. In winter and early spring, there is a greater frequency of days with the influence of
77 high-pressure systems that hinder the passage of cold fronts, favoring the formation of a high-
78 intensity heat island, which generates more appropriate conditions for the occurrence of high
79 pollutant concentration events [19].

80
81

82



83
84

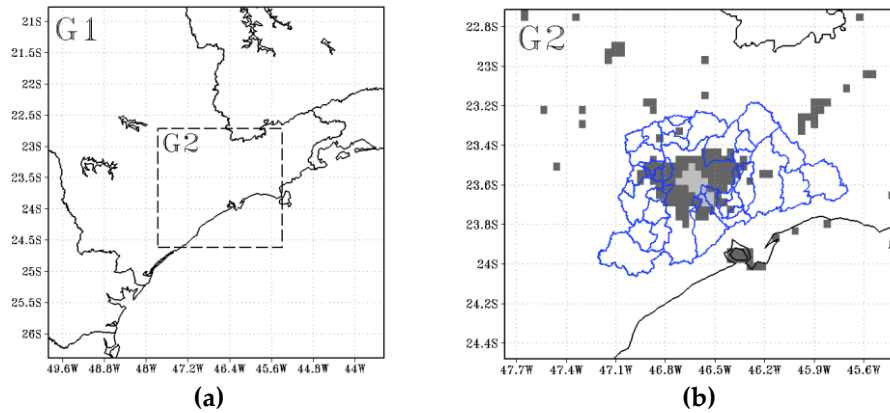
Figure 1. Location and topography map of the MASP. Scale color bar in meters.

85 **2.2. SPM-BRAMS**

86 In this work, the version 3.2 of the BRAMS model (*Brazilian Development on Regional Atmospheric*
87 *Modeling System*, [20]) was used, which is based on the Regional Atmospheric Modeling System
88 (RAMS, [21]). The model allows simulating several spatial scales, integrating the microscale with the
89 larger scales. The system of equations that governs the atmospheric state is solved using second-order
90 finite difference schemes, both in time and space. The conservation of mass, moment, and energy in
91 the model is guaranteed since the advection terms of these equations are treated in flow. Numerical
92 instability is minimized by using smaller time steps in solving equations in higher resolution grids.
93 Atmospheric physical processes not explicitly resolved by the model are parameterized. The model
94 has a multiple grid scheme that allows the simultaneous resolution of the equations. The interaction
95 processes between the surface and atmosphere are carried out at BRAMS using the LEAF-3 model
96 (Land Ecosystem-Atmosphere Feedback model version 3, [22]) for vegetated areas and with TEB
97 (Town Energy Budget, [23]) for urban areas.

98 Figure 2 presents the nesting grids used in the simulations centered at MASP (-23.60°, -46.65°).
99 The horizontal spacing grid of both domains is 16 and 4 km, from lower to the higher resolution. For
100 the topography, files with spacing between 1 km grid points provided by the United States Geological
101 Survey (USGS) were used. For the sea water surface temperature, weekly mean values corresponding
102 to the simulated periods were used as input data, without considering the update of these files during
103 the rounds. As input meteorological data, the Global Forecasting System (GFS) global model's
104 outputs with a horizontal spacing grid of 1° were used. For all analysis of the results, the simulations
105 were run one day before the nocturnal event, and we reject the first 24 hours to avoid the spin-up
106 effect [24] of the meteorological part of the model and to allow the model to accumulate more realistic
107 amounts of pollutants in the atmosphere. The first level of the model output considered is 33.4 m

108 above the surface. The model physics and land use parameterization configuration are the same as
109 Morais et al. [25].
110



111
112
113

114 **Figure 2.** Grid domains used in the simulation. (a) Lower resolution domain (G1), and (b) higher
115 resolution. Lighter gray color represents the dense urban area since dark gray is the suburban area
116 (similar to Morais et al. [25]).

117 The Simple Photochemical Module (SPM, [26]) was inserted in the BRAMS model to generate
118 operational forecasts of ozone concentrations and other constituents for the MASP with only 15
119 chemical reactions. Ozone formation was represented without considering hydrocarbon speciation.
120 These equations were selected from the chemical mechanism SAPRC-99, which in turn is used in the
121 CIT photochemical model (Caltech Institute of Technology, [27]). Volatile organic compounds are
122 considered in a single category to simplify the numerical scheme and reduce the calculation time.
123 The emissions module consists of an Eulerian dispersion model integrating the mass conservation
124 equation, which distributes the emission. For vehicular emission, the emission is still distributed in
125 space and time within the grid following a daily cycle based on in a Gaussian pair to represent the
126 times with the highest flow vehicular. The module also makes an adjustment to consider variations
127 in emissions during the week and on weekends. The same parameterization solves the terms of
128 advection and turbulent transport of pollutants as the model.

129 2.3. Model Evaluation

130 In this work, two statistical indices were used to assess the proximity of the result generated by
131 the model with the observed values of O₃ in the MASP. The Bias (or mean error) measures the model's
132 tendency to underestimate or overestimate the value of a variable with its observed value and is
133 defined by the expression,

$$BIAS = \frac{1}{N} \sum_{i=1}^N (S_i - O_i), \quad (1)$$

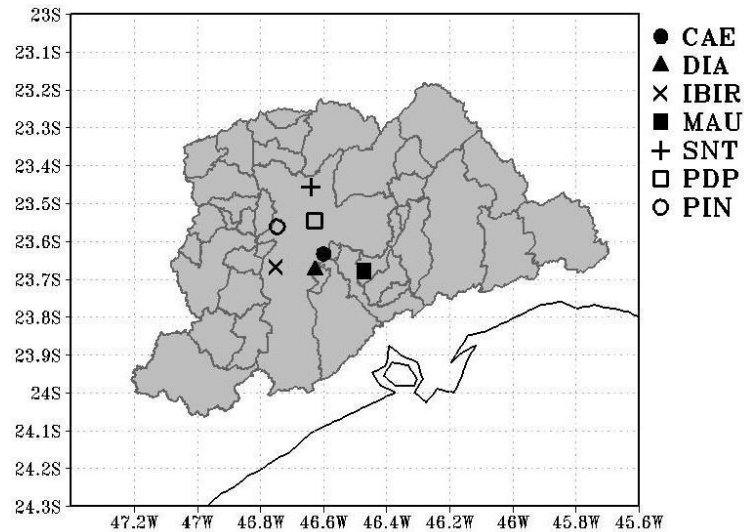
134 where S_i corresponds to the i -th value of the simulated, and O_i for the same observed variable. N is
135 the number of data.

136 The Root Mean Square Error (RMSE) is used to express the accuracy of the numerical results and
137 is given by the following equation

$$RMSE = \frac{1}{N} \sum_{i=1}^N \sqrt{(S_i - O_i)^2}, \quad (2)$$

138 where S_i corresponds to the i -th value of the simulated, and O_i for the same observed variable. N is
139 the number of data.

140 Some representative points of CETESB's pollutant monitoring stations were chosen to assess the
141 model's performance in representing the concentration at levels close to the surface. The location of
142 these points is shown in Figure 3. For meteorological variables, the model was extensively validated
143 by Morais et al. [25,28].
144



145
146 **Figure 3.** Location of CETESB's monitoring network stations in the Metropolitan Region of São Paulo
147 (in gray) used for this study, where CAE corresponds to São Caetano do Sul station, DIA to Diadema
148 station, IBI to Parque do Ibirapuera station, MAU to Mauá station, SNT to Santana station, PDP to
149 Parque Dom Pedro II station and PIN to Pinheiros station.

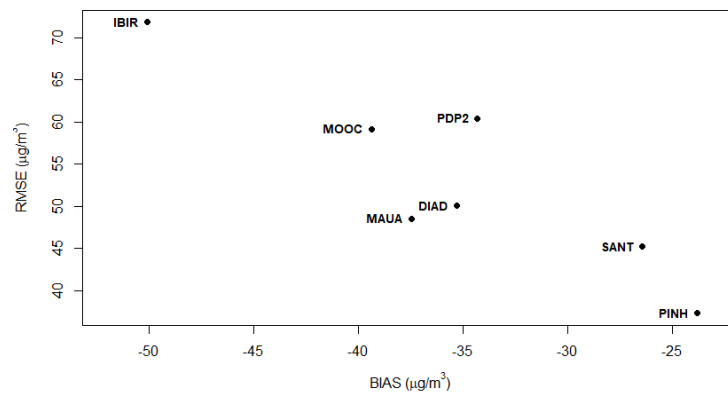
150 2.4. Experimental design

151 Two different periods were considered to study the local meteorological factors that influence the
152 increase in nocturnal ozone concentration. The first one corresponds to the condition where the
153 nighttime ozone increase was recorded in all stations (case 7E), which was occurred on 25th December
154 2010. The second was considered a period where it was not recorded nocturnal ozone in any of the
155 selected stations (case 0E). The last one was on 22nd January 2005. The discussion was done analyzing
156 the O_3 evolution in each station and by an average nocturnal concentration map. After, a vertical profile
157 of the ozone is done, considering the latitude of MASP.

158 3. Results and Discussions

159 3.1. Model Evaluation

160 Figure 4 shows a scatter plot of the RMSE and BIAS of the ozone concentration for all air quality
161 stations in MASP. By BIAS, it appears that the model tends to underestimate the values of O_3 . The
162 absolute value of these indices is related to the order of magnitude of the variable. However, it
163 appears that the values are like those obtained by other authors [6,29]. Besides, it is noted that the
164 Ibirapuera park station has the worst rates, which may be related to the intense presence of green
165 areas in the place, needing to improve this type of representation in the model [30].



166

167

168

169

Figure 4. RMSE versus BIAS for ozone concentration. Each point represents an air quality station in the MASP: São Caetano do Sul (CAET), Diadema (DIAD), Ibirapuera Park (IBIR), Mauá (MAUA), Pq. D. Pedro II (PDP2), Pinheiros (PINH) and Santana (SANT).

170

3.2. Nocturnal Ozone experiments

171

3.2.1. No increase in ozone concentration (0E)

172

173

174

175

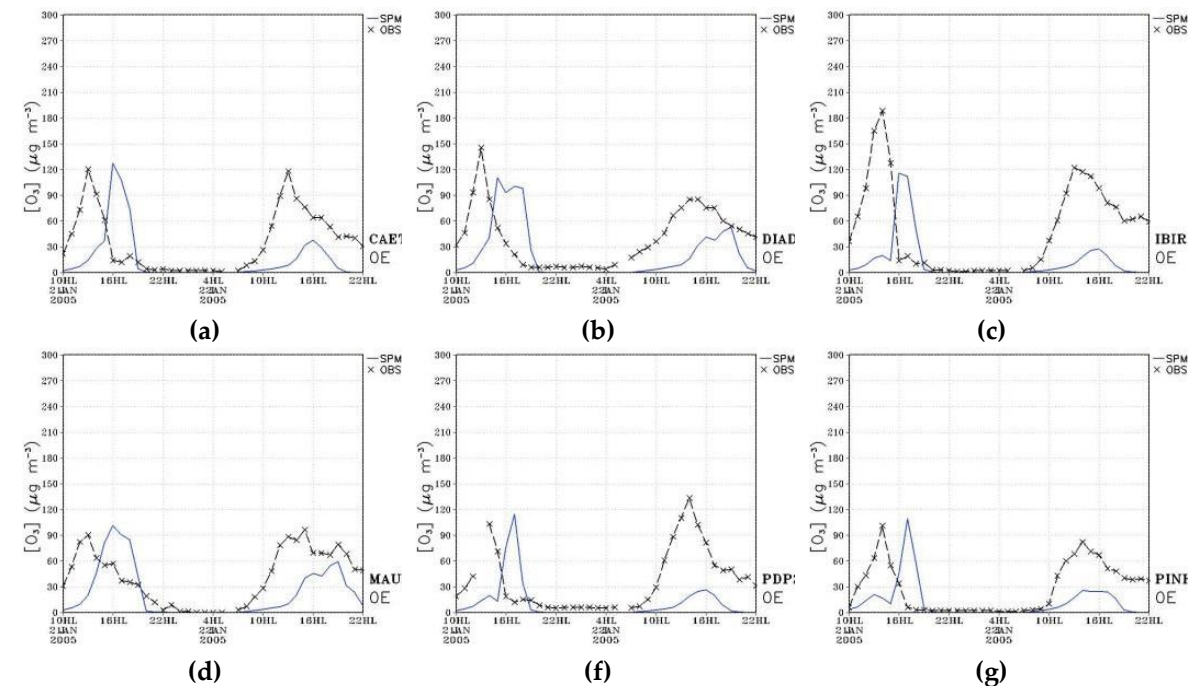
176

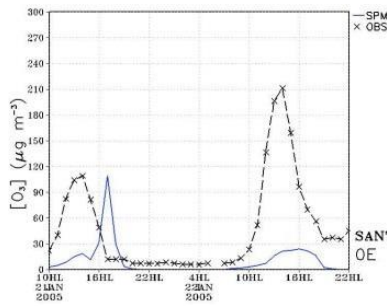
177

178

179

180

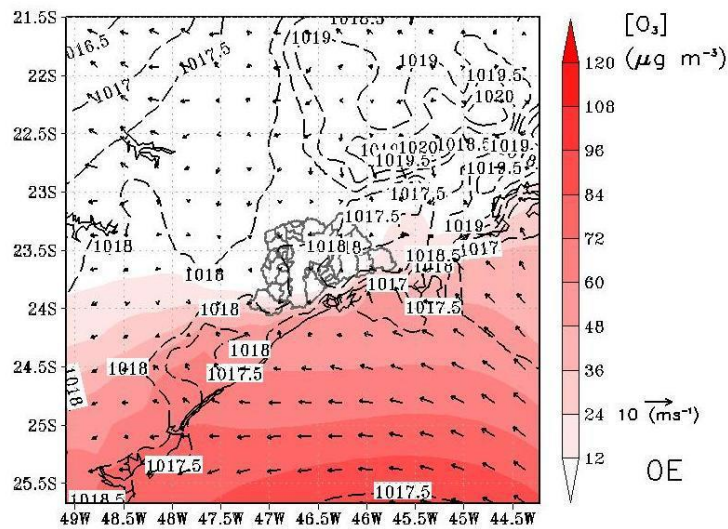




(h)

Figure 5. Ozone concentration (in $\mu\text{g m}^{-3}$) measurement (OBS, with x black) and simulated (SPM, blue line) for (a) São Caetano do Sul (CAET), (b) Diadema (DIAD), (c) Ibirapuera Park (IBIR), (d) Mauá (MAUA), (e) Pq. D. Pedro II (PDP2), (f) Pinheiros (PINH) and (g) Santana (SANT).

181



182

183

184

185

Figure 6. Average ozone concentration (color bar, in $\mu\text{g m}^{-3}$), reduced pressure at average sea level (hPa), and average wind (m s^{-1}) for the corresponding period between 22 HL and 10 HL (Local Time) at the first output level of the model.

186

3.2.2. Increase in ozone concentration (7E)

187

188

189

190

191

192

193

194

195

196

In the 7E case (Figure 7), the model represented the nocturnal increase in ozone, although, in most seasons, an underestimation occurred (difference of almost $30 \mu\text{g m}^{-3}$). At Diadema and Parque Dom Pedro II stations, although the nocturnal increase in ozone has been represented, there is a lag in the model's concentration and that obtained in such stations. Regarding daytime maximums, there was an overestimation for both days at all points analyzed. The average ozone field for this simulation (Figure 8) showed values below $24 \mu\text{g m}^{-3}$ in the continental part and a core of maximum values southwest of the domain, where the wind tends to have a higher average intensity when compared the rest of the study area.

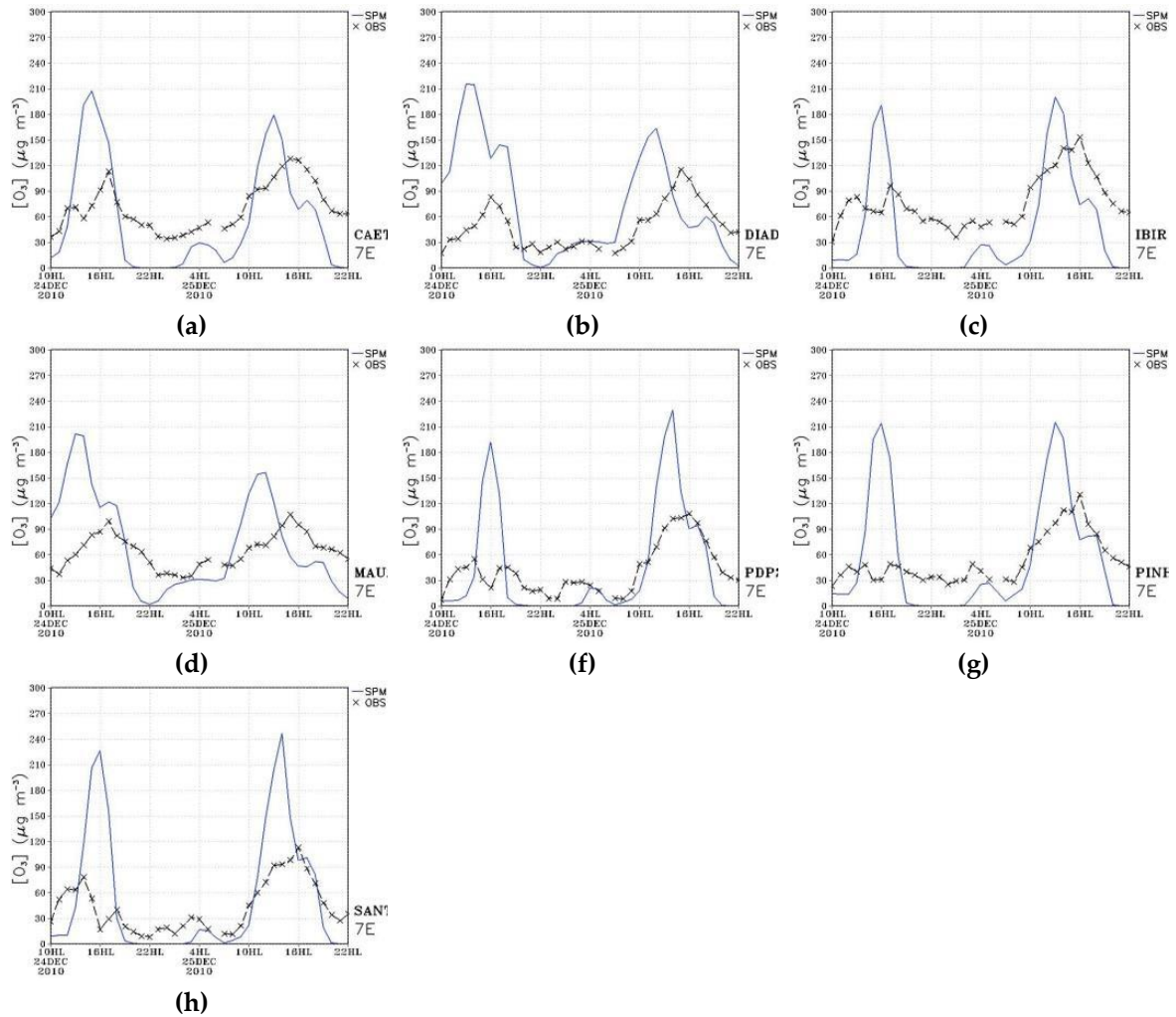


Figure 7. Ozone concentration (in $\mu\text{g m}^{-3}$) measurement (OBS, with x black) and simulated (SPM, blue line) for (a) São Caetano do Sul (CAET), (b) Diadema (DIAD), (c) Ibirapuera Park (IBIR), (d) Mauá (MAUA), (e) Pq. D. Pedro II (PDP2), (f) Pinheiros (PINH) and (g) Santana (SANT).

197

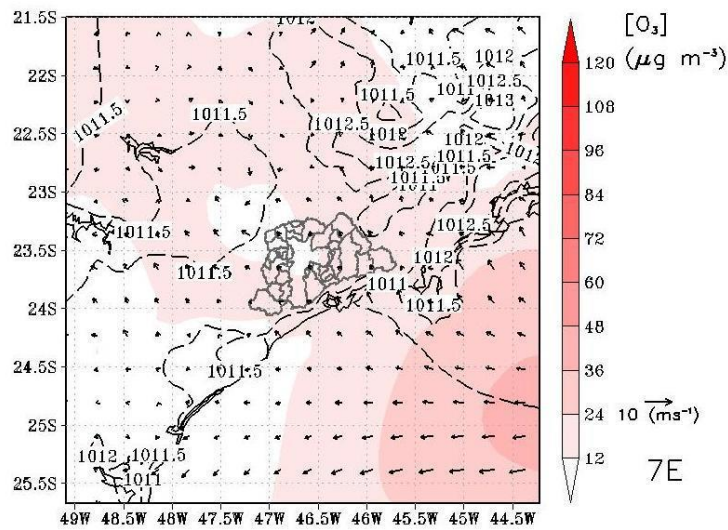


Figure 8. Average ozone concentration (color bar, in $\mu\text{g m}^{-3}$), reduced pressure at average sea level (hPa), and average wind (m s^{-1}) for the corresponding period between 22 HL and 10 HL (Local Time) at the first output level of the model.

198
 199
 200
 201
 202

203 3.2.3. Ozone vertical profile

204 In case 0E (Figure 9), the wind remains weak throughout the period, with a minimal vertical
205 component. The atmosphere under the MASP is clean for all hours of the night. When an increase in
206 the concentration of ozone is observed in all stations in the MASP (case 7E, Figure 10), the sub-wind
207 component is more intense than when this phenomenon is observed in only a few stations. This result
208 shows that, in the cases of the nocturnal peak, the vertical transport of ozone present in the residual
209 layer has an essential contribution in the generation of increased concentration at levels close to the
210 surface.

211

212

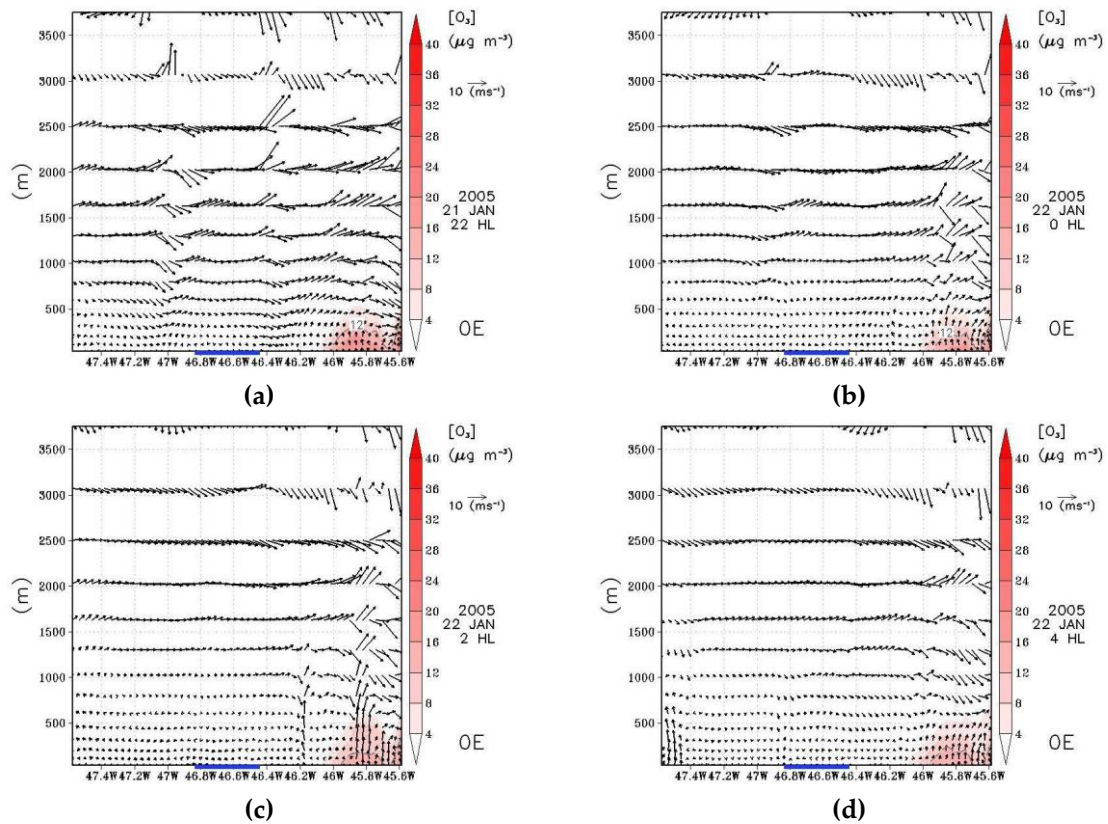


Figure 9. Ozone concentration ($\mu\text{g m}^{-3}$) and vertical wind component (m s^{-1}) with the zonal wind (m s^{-1}) for a vertical view at 23.616°S latitude, for the case 0E. The blue line indicates the location of the MASP. Local Time is indicated in the corresponding figure.

213

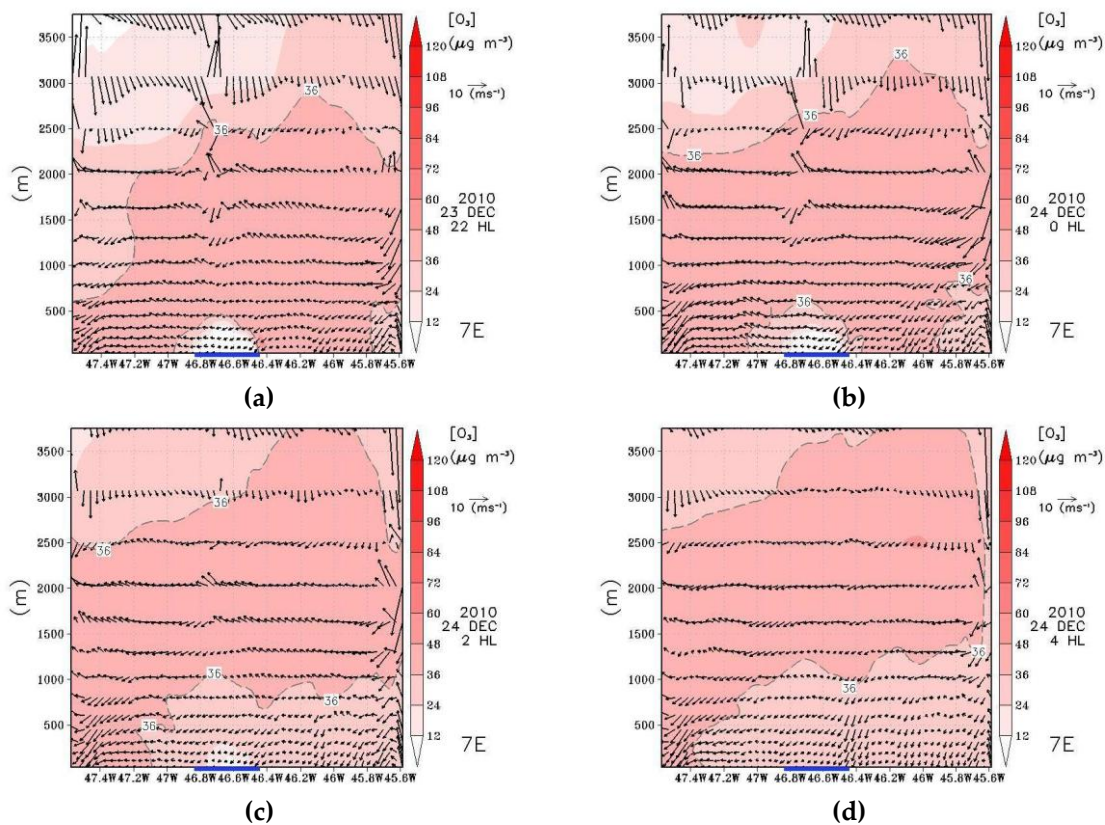


Figure 10. Ozone concentration ($\mu\text{g m}^{-3}$) and vertical wind component (m s^{-1}) with the zonal wind (m s^{-1}) for a vertical view at 23.616° S latitude, for the case 7E. The blue line indicates the location of the MASP. Local Time is indicated in the corresponding figure.

214 **4. Conclusions and Remarks**

215 To study at a local level the characteristics that contributes to an increase in nocturnal ozone
 216 concentrations in the MASP, two cases were simulated, when no increase is observed (0E) and when
 217 the secondary peak is observed in all air quality stations (7E). In general, the model was able to better
 218 represent the nocturnal evolution of ozone concentrations close to the surface at stations located in
 219 the MASP. For daytime concentrations, the model simulated concentrations with the maximum
 220 values overestimated. The atmospheric condition resulting from the simulations for MASP was
 221 similar, confirming that the formation of nightly ozone peaks is not linked to the synoptic situation
 222 in this study region. In this case, the greatest influence resides in the amount of ozone that is trapped
 223 in the residual layer and the intensity of the subsiding currents over the urban area, as seen in the
 224 vertical sections for all cases.

225 **Author Contributions:** All authors have contributed equally. All authors have read and agreed to the published
 226 version of the manuscript.

227 **Funding:** The authors would like to thank the financial support of the Coordenação de Aperfeiçoamento de
 228 Pessoal de Nível (CAPES) and the São Paulo Research Foundation (#2011/01040-0).

229 **Conflicts of Interest:** The authors declare no conflict of interest.

230 **References**

231 1. Liana, M.; Edison, O.; Jorge, M.; Marcos, M.; Leda, A.; Guerrero, U.; Leila, M.D. Current state of air
 232 quality in major cities of Latin America. *Ciência e Nat.* **2016**, *38*, 523–531, doi:10.5902/2179460X20290.
 233 2. Patz, J.A.; Campbell-Lendrum, D.; Holloway, T.; Foley, J.A. Impact of regional climate change on human
 234 health. *Nature* **2005**, *438*, 310–317, doi:10.1038/nature04188.

- 235 3. Woodall, G.M.; Hoover, M.D.; Williams, R.; Benedict, K.; Harper, M.; Soo, J.C.; Jarabek, A.M.; Stewart,
236 M.J.; Brown, J.S.; Hulla, J.E.; et al. Interpreting mobile and handheld air sensor readings in relation to air
237 quality standards and health effect reference values: Tackling the challenges. *Atmosphere (Basel)*. **2017**, *8*,
238 doi:10.3390/atmos8100182.
- 239 4. Bell, M.L.; Zanobetti, A.; Dominici, F. Who is More Affected by Ozone Pollution? A Systematic Review
240 and Meta-Analysis. *Am. J. Epidemiol.* **2014**, *180*, 15–28, doi:10.1093/aje/kwu115.
- 241 5. Wang, T.; Kwok, J.Y.H. Measurement and Analysis of a Multiday Photochemical Smog Episode in the
242 Pearl River Delta of China. *J. Appl. Meteorol.* **2003**, *42*, 404–416, doi:10.1175/1520-
243 0450(2003)042<0404:MAAOAM>2.0.CO;2.
- 244 6. Andrade, M.D.F.; Ynoue, R.Y.; Freitas, E.D.; Todesco, E.; Vara Vela, A.; Ibarra, S.; Martins, L.D.; Martins,
245 J.A.; Carvalho, V.S.B. Air quality forecasting system for Southeastern Brazil. *Front. Environ. Sci.* **2015**, *3*,
246 1–14, doi:10.3389/fenvs.2015.00009.
- 247 7. Samaali, M.; Moran, M.D.; Bouchet, V.S.; Pavlovic, R.; Cousineau, S.; Sassi, M. On the influence of
248 chemical initial and boundary conditions on annual regional air quality model simulations for North
249 America. *Atmos. Environ.* **2009**, *43*, 4873–4885, doi:10.1016/J.ATMOSENV.2009.07.019.
- 250 8. Balzarini, A.; Pirovano, G.; Honzak, L.; Žabkar, R.; Curci, G.; Forkel, R.; Hirtl, M.; San José, R.; Tuccella,
251 P.; Grell, G.A. WRF-Chem model sensitivity to chemical mechanisms choice in reconstructing aerosol
252 optical properties. *Atmos. Environ.* **2015**, *115*, 604–619, doi:10.1016/J.ATMOSENV.2014.12.033.
- 253 9. Vara-Vela, A.; Andrade, M.F.; Kumar, P.; Ynoue, R.Y.; Muñoz, A.G. Impact of vehicular emissions on
254 the formation of fine particles in the Sao Paulo Metropolitan Area: A numerical study with the WRF-
255 Chem model. *Atmos. Chem. Phys.* **2016**, *16*, 777–797, doi:10.5194/acp-16-777-2016.
- 256 10. Romero, H.; Ihl, M.; Rivera, A.; Zalazar, P.; Azocar, P. Rapid urban growth, land-use changes and air
257 pollution in Santiago, Chile. *Atmos. Environ.* **1999**, *33*, 4039–4047, doi:10.1016/S1352-2310(99)00145-4.
- 258 11. Mar, K.A.; Ojha, N.; Pozzer, A.; Butler, T.M. Ozone air quality simulations with WRF-Chem (v3.5.1) over
259 Europe: Model evaluation and chemical mechanism comparison. *Geosci. Model Dev. Discuss.* **2016**, *1*, 1–
260 50, doi:10.5194/gmd-2016-131.
- 261 12. Ren, X.; Mi, Z.; Georgopoulos, P.G. Comparison of Machine Learning and Land Use Regression for fine
262 scale spatiotemporal estimation of ambient air pollution: Modeling ozone concentrations across the
263 contiguous United States. *Environ. Int.* **2020**, *142*, 105827, doi:10.1016/j.envint.2020.105827.
- 264 13. Gramsch, E.; Cereceda-Balic, F.; Oyola, P.; von Baer, D. Examination of pollution trends in Santiago de
265 Chile with cluster analysis of PM10 and Ozone data. *Atmos. Environ.* **2006**, *40*, 5464–5475,
266 doi:10.1016/J.ATMOSENV.2006.03.062.
- 267 14. Khan, B.A.; de Freitas, C.R.; Shooter, D. Application of synoptic weather typing to an investigation of
268 nocturnal ozone concentration at a maritime location, New Zealand. *Atmos. Environ.* **2007**, *41*, 5636–5646,
269 doi:10.1016/j.atmosenv.2007.02.040.
- 270 15. Alp, K.; Hanedar, A.O. Determination of transport processes of nocturnal ozone in Istanbul atmosphere.
271 *Int. J. Environ. Pollut.* **2009**, *39*, 213, doi:10.1504/IJEP.2009.028686.
- 272 16. Zhu, X.; Ma, Z.; Li, Z.; Wu, J.; Guo, H.; Yin, X.; Ma, X.; Qiao, L. Impacts of meteorological conditions on
273 nocturnal surface ozone enhancement during the summertime in Beijing. *Atmos. Environ.* **2020**, *225*,
274 117368, doi:10.1016/j.atmosenv.2020.117368.
- 275 17. IBGE Censo Demográfico: Características da população – amostra.
- 276 18. Nair, K.N.; Freitas, E.D.; Sánchez-Ccoyllo, O.R.; Silva Dias, M. a. F.; Silva Dias, P.L.; Andrade, M.F.;

- 277 Massambani, O. Dynamics of urban boundary layer over São Paulo associated with mesoscale processes.
278 *Meteorol. Atmos. Phys.* **2004**, *86*, 87–98, doi:10.1007/s00703-003-0617-7.
- 279 19. Andrade, M. de F.; Kumar, P.; de Freitas, E.D.; Ynoue, R.Y.; Martins, J.; Martins, L.D.; Nogueira, T.;
280 Perez-Martinez, P.; de Miranda, R.M.; Albuquerque, T.; et al. Air quality in the megacity of São Paulo:
281 Evolution over the last 30 years and future perspectives. *Atmos. Environ.* **2017**, *159*, 66–82,
282 doi:10.1016/j.atmosenv.2017.03.051.
- 283 20. Freitas, S.R.; Panetta, J.; Longo, K.M.; Rodrigues, L.F.; Moreira, D.S.; Rosário, N.E.; Silva Dias, P.L.; Silva
284 Dias, M.A.F.; Souza, E.P.; Freitas, E.D.; et al. The Brazilian developments on the Regional Atmospheric
285 Modeling System (BRAMS 5.2): an integrated environmental model tuned for tropical areas. *Geosci.*
286 *Model Dev.* **2017**, *10*, 189–222, doi:10.5194/gmd-10-189-2017.
- 287 21. Cotton, W.R.; Pielke Sr., R. a.; Walko, R.L.; Liston, G.E.; Tremback, C.J.; Jiang, H.; McAnelly, R.L.;
288 Harrington, J.Y.; Nicholls, M.E.; Carrio, G.G.; et al. RAMS 2001: Current status and future directions.
289 *Meteorol. Atmos. Phys.* **2003**, *82*, 5–29, doi:10.1007/s00703-001-0584-9.
- 290 22. Walko, R.L.; Band, L.E.; Baron, J.; Kittel, T.G.F.; Lammers, R.; Lee, T.J.; Ojima, D.; Pielke, R.A.; Taylor,
291 C.; Tague, C.; et al. Coupled Atmosphere–Biophysics–Hydrology Models for Environmental Modeling.
292 *J. Appl. Meteorol.* **2000**, *39*, 931–944, doi:10.1175/1520-0450(2000)039<0931:CABHMF>2.0.CO;2.
- 293 23. Masson, V. A physically-based scheme for the urban energy budget in atmospheric models. *Boundary-*
294 *Layer Meteorol.* **2000**, *94*, 357–397.
- 295 24. *Atmospheric Data Analysis*; Daley, R., Ed.; Cambridge University Press: Cambridge, UK, 1991;
- 296 25. Morais, M.V.B.; Freitas, E.D.; Marciotto, E.R.; Urbina Guerrero, V.V.; Martins, L.D.; Martins, J.A.
297 Implementation of observed sky-view factor in a mesoscale model for sensitivity studies of the urban
298 meteorology. *Sustain.* **2018**, *10*, doi:10.3390/su10072183.
- 299 26. Freitas, E.D.; Martins, L.D.; Silva Dias, P.L.; Andrade, M.F. A simple photochemical module
300 implemented in RAMS for tropospheric ozone concentration forecast in the metropolitan area of São
301 Paulo, Brazil: Coupling and validation. *Atmos. Environ.* **2005**, *39*, 6352–6361,
302 doi:10.1016/j.atmosenv.2005.07.017.
- 303 27. Wang, L.; Zhang, Y.; Wang, K.; Zheng, B.; Zhang, Q.; Wei, W. Application of Weather Research and
304 Forecasting Model with Chemistry (WRF/Chem) over northern China: Sensitivity study, comparative
305 evaluation, and policy implications. *Atmos. Environ.* **2014**, doi:10.1016/j.atmosenv.2014.12.052.
- 306 28. Morais, M.V.B. de; Freitas, E.D. de; Urbina Guerrero, V.V.; Martins, L.D. A modeling analysis of urban
307 canopy parameterization representing the vegetation effects in the megacity of São Paulo. *Urban Clim.*
308 **2016**, *17*, 102–115, doi:10.1016/j.uclim.2016.04.004.
- 309 29. Pellegatti Franco, D.M.; Andrade, M. de F.; Ynoue, R.Y.; Ching, J. Effect of Local Climate Zone (LCZ)
310 classification on ozone chemical transport model simulations in Sao Paulo, Brazil. *Urban Clim.* **2019**, *27*,
311 293–313, doi:10.1016/j.uclim.2018.12.007.
- 312 30. Morais, M.V.B. de; Freitas, E.D. de; Urbina Guerrero, V.V.; Martins, L.D. A modeling analysis of urban
313 canopy parameterization representing the vegetation effects in the megacity of São Paulo. *Urban Clim.*
314 **2016**, *17*, 102–115, doi:10.1016/j.uclim.2016.04.004.
- 315

